

Anodization for 2024 Al Alloy from Sulfuric-Citric Acid and Anticorrosion Performance of Anodization Films

Meng xiangfeng¹, Wei Guoying^{1,*}, Ge Hongliang¹, Yu Yundan¹, Cao ying¹, Horst Dettinger²

¹ College of Materials Science & Engineering, China Jiliang University, HangZhou 310018, China

² ZEH Company, Stuttgart, Germany

*E-mail: guoyingwei@sina.com.cn

Received: 13 June 2013 / Accepted: 22 July 2013 / Published: 1 August 2013

Porous anodic alumina has been obtained through anodic oxidation in a mixed solution of sulfuric acid and citric acid. Potentiodynamic polarization and electrochemical impedance spectroscopy of anodization film have been studied in a 3.5wt.% NaCl solution, which were conducted to assess the corrosion resistance of the anodized film. The voltage-time curve shows that the oxidation voltage changes from 0 V to 8.6 V dramatically, and then decreases to a steady value(7.7V) when the oxidation time reaches to 300s. The anodic polarization curves shows that corrosion potential of the anodized film is -0.7 V vs Ag/AgCl, which is more positive than that of the 2024 Al alloy. Corrosion potential of the anodized film sealed by nickel and cobalt salt is -0.4V vs Ag/AgCl. Corrosion results indicated that the capacitance of corrosion reaction was changed with the increase of oxidation time. Inerratic nanopores appeared on the surface of the 2024 Al alloy from the SEM results. We also found that the pores size increased gradually with the oxidization time. γ -Al₂O₃, α -Al₂O₃ and a small amount of amorphous phase for anodization film appeared from the X-ray diffraction (XRD) pattern.

Keywords: 2024 Al alloy; anodization; sulfuric-citric mixed acid; potentiodynamic polarization; EIS

1. INTRODUCTION

Aluminium alloys are widely used in the fields of aerospace and automotive industries due to their excellent properties, such as strengthen and good formability. Unfortunately, aluminium alloys are susceptible to corrosion, which greatly restricts their applications, especially in some corrosive circumstances. Anodization is a very common method for preparing the anodic oxide film. Porous anodic alumina films can be generated by aluminium anodization in aqueous electrolytes. Some researchers have found that properties of anodization films can be tailored by selecting the anodizing conditions. In this way, we can obtain ordered templates [1–5], corrosion [6–8] or wear resistant layers

and colored surfaces [9–12]. Alumina nanostructures are normally fabricated using an electrochemical etching process in which the pores grow perpendicularly to a planar surface in a highly ordered hexagonal “honeycomb” structure [13]. The characteristics of porous alumina films, such as pore diameters and corrosion resistance, strongly depended on the chosen electrolyte and the duration of anodization.

Anti-corrosion properties of conventional anodized aluminium alloys have been extensively investigated using electrochemical impedance spectroscopy (EIS) [14–22]. Therefore, the corrosion resistance of anodic oxidation film can be deduced according to the Bode and Nyquist plots, which obtained from the experiment. Meanwhile the experiments showed that the protection efficiency strongly depended on the porosity of the porous anodic alumina films [11–12].

The aim of this present work is to investigate the oxidation time on the characteristics and performance of the anodization film from the sulfuric-citric acid anodizing system, especially the electrochemical characteristics. Potentiodynamic polarization, electrochemical impedance spectroscopy, voltage-time characteristic, SEM, XRD and Thickness are researched through this article.

2. EXPERIMENTAL PART

2.1 Materials and coating preparation

The 2024 Al alloy was used in the experiment, which the nominal composition shown in the Table 1. The specimens, 6cm×2cm×5mm in dimensions, were need to three steps of pretreatment. Oxide first, the aluminum samples thus obtained were chemically immersed in the 32g/L P3 Almeco 36 at 65° C for 10min to remove the grease and were immediately rinsed with distilled water; the second step, we put the first-step samples into 44g/L TURCO Aluminetch 2 at 60° C for 2min to remove the nature oxide layer and were immediately rinsed with distilled water, we can find the surface of the aluminum alloy changed into black, so, the samples were immersed in the 35ml/L TURCO Liquid Smut Go NC at 50° C for 10min to remove the black layer, ultrasonically washed with distilled water, finally dried for oxidation.

Electrolyte was prepared from the solution of citric acid (153.6g/L) and 98 % sulfuric acid(8ml/L), and the electrical parameters were fixed as follows: voltage 16V, temperature 37° C, and the time of anodic oxidation was from 5min to 60min.

Table 1. Composites of 2024 Al alloy (wt. %).

Cu	Mg	Mn	Fe	Si	Zn	Ti	Cr	Al
4.36	1.49	0.46	0.25	0.14	0.07	0.01	<0.01	Bal.

2.2 Electrochemical tests

Electrochemical behaviours were carried out in a nitrogen atmosphere glove box system filled with dry nitrogen. Voltage-time curves for anodizing Al 2024 alloy, potentiodynamic polarisation and

EIS measurements for the samples were performed using an electrochemical workstation (PARSTAT 2273) in sulfuric-citric acid at room temperature. All these electrochemical experiments were carried out in a three electrode system.

Potentiodynamic polarization and EIS measurements were carried out in a 3.5 wt. % NaCl solution, which used as the corrosive medium. Porous anodic alumina was used as working electrode (WE), which exposed to solution was approximately 1cm². Saturated calomel electrode (SCE) was used as the reference electrode, and a platinum plate was used as the counter electrode (CE). Scanning rate of potentiodynamic polarisation measurements was varying from 0.5mv/s to 4mv/s. EIS measurements were performed in a range of 0.01 Hz and 100 kHz.

3. RESULTS AND DISCUSSION

3.1 Electrochemical behavior

3.1.1 Chrono-potentiometric measurements

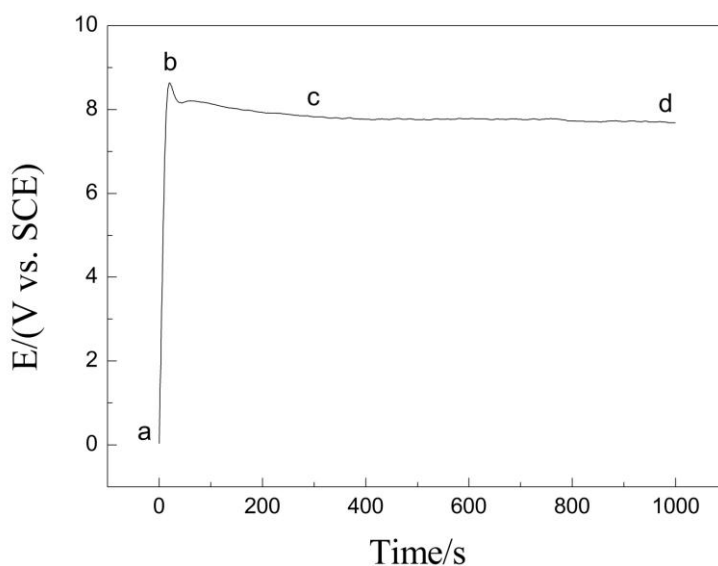


Figure 1. Voltage-time curves of 2024 Al alloy in sulfuric-citric acid solution (153.6g/L citric acid and 8ml/L 98% sulfuric acid) Temperature: 298 K.

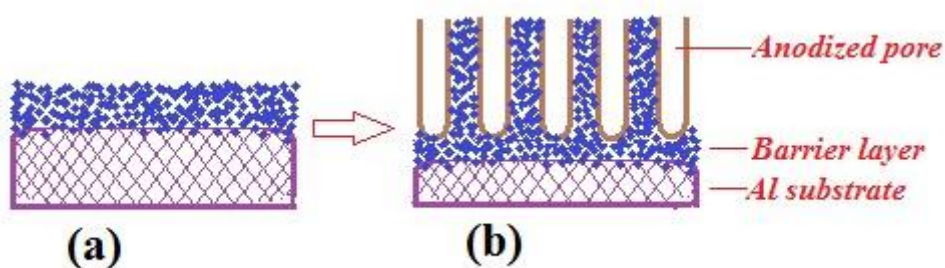


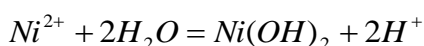
Figure 2. Schematic diagram of the generation of anodic oxidation film on 2024 Al alloy.

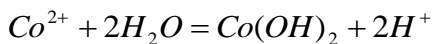
Voltage–time curves for anodizing Al 2024 alloy in sulfuri-citric acid at 40 mA cm^{-2} are shown in Fig. 1. The general form of all responses follows the expected shape for formation of the porous alumina at constant current density. The classic response of anodization at constant current density [24] shows an approximately linear increase with voltage from the commencement of anodization, i.e. a barrier oxide layer starts to grow. The ab segment is the formation of the barrier layer in Fig1. The voltage changes sharply from zero to the maximum from the beginning to 20 seconds. And the voltage of reaction reaches 8.6V, which called critical voltage. The results showed that a continuous non-porous layer formed on the anode surface, which prevents the continued thickening of the layer. The thickness of the barrier layer is proportional to the oxidation voltage. However, there's an inverse relationship between the thickness of the barrier layer and the rate of dissolution in the electrolyte. The bc segment is the stage of the formation of porous layer. The oxidation voltage decreases after the voltage reaches the maximum value with a decrease of the maximum value of 10%-15%. It showed that the non-porous barrier layer began to be dissolved in the electrolyte. Meanwhile, the porous layer began generating. The cd segment reflects that the thickness of the porous layer increase slowly. After anodizing for approximately 300s, the oxidation voltage began to reach a stationary value. Therefore, the steady-state voltage corresponds to a dynamic equilibrium between film growth and dissolution in the electrolyte. When the steady state corresponds to a dynamic equilibrium, the thickness of the anodization films cannot change[24]. In order to express the growth of the anodization film on the surface of 2024 Al alloy vividly, we make a schematic diagram showed in Fig.2 according to the above results. The barrier layer formed gradually on the 2024Al alloy as described on Fig.2a. The non-porous barrier layer began to be dissolved in the electrolyte. Meanwhile, the porous layer began generating as showed from Fig2b.

3.1.2 Potentiodynamic polarization study

Fig. 3 shows the corrosion potential of the anodizing film moved to negative potential with oxidation time in the early stage. After 30 minutes, the corrosion potential of the anodization film moved to a more positive potential -0.767V. As time proceeds, corrosion potential of the anodization film increases. The corrosion potential of anodized film increased to -0.715V under the oxidation time of 50min.

Figure 4 shows considerable change in the corrosion potential of the anodized samples and 2024 Al alloy. The corrosion potential of the oxide films and the anodization film sealed by nickel and cobalt salt for 40 min are significantly lower than that of the 2024 Al alloy. Corrosion potential of 2024Al alloy is -1.13V vs. Ag/AgCl(curve a in Fig 4); Corrosion potential of anodization film is -0.72V vs. Ag/AgCl(curve b in Fig 4); corrosion potential of anodization film sealed by nickel and cobalt salt solution is -0.48V vs. Ag/AgCl(curve c in Fig 4). The sequence of corrosion was: sealed anodization film > anodization film > 2024 Al according to the above results. In order to research the potentiodynamic polarization results, the reaction mechanism of an aluminum anodic film should be discussed. It maybe comes from a series of chemical reaction during the sealing behavior of anodization film at 100°C nickel-cobalt salt solution:





The micropores of the anodization film are filled by nickel hydroxide and cobalt hydroxide. As the anodization film is composed of the inner denser barrier layer and outer looser porous layer, only the chloride ions can reach the bottom of the barrier layer and erode the denser anodization film through the porous in a solution of 3.5 wt.% NaCl.

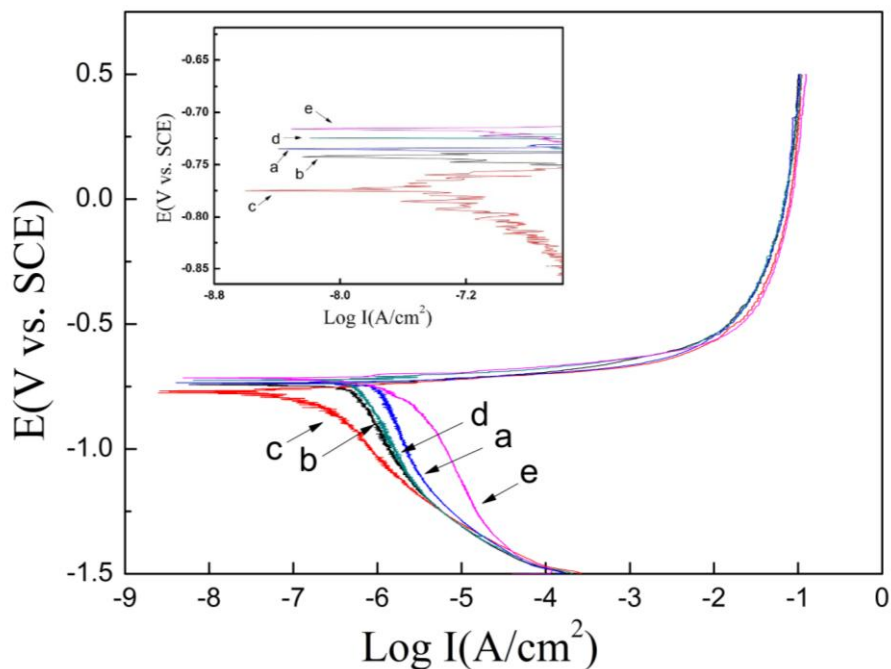


Figure 3. Polarization curves of anodic oxidation film with different anodizing times. Temperature: 298K; Voltage: 16V. (a) 10min; (b) 20min (c) 30min (d) 40min (e) 50min.

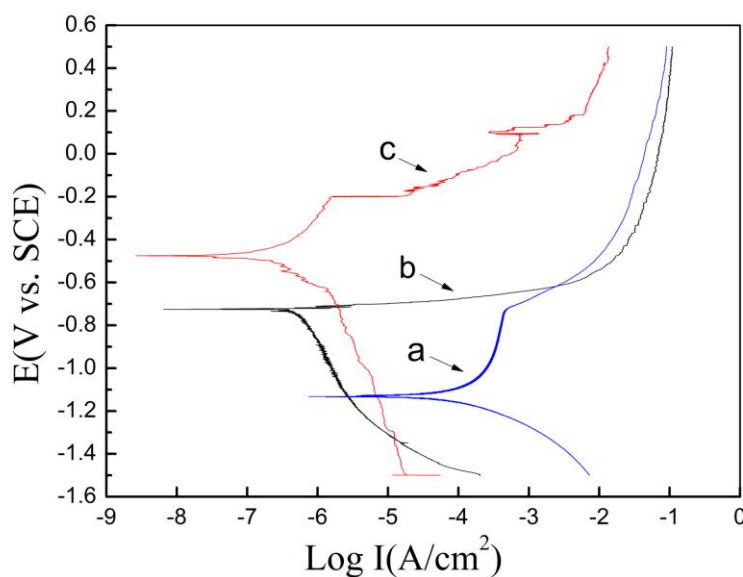


Figure 4. Polarization curves of (a) 2024 Al alloy (b) anodization film (40min) (c) sealed by nickel and cobalt salt solution for 40min after 20min of immersion in a 3.5wt. % NaCl solution. Temperature: 298K. Scan rate: 1mv/s.

When the chloride ion gathered at the bottom of the porous and reached a certain level, the barrier layer begins to dissolve. The porous will obstruct the transfer processes of aggressive ions. The anodic anodization film obtained will undergo a sealing behavior and more porous are completely or partially sealed. Both the speed of chloride ions reaches the barrier layer and the amount of chloride ions aggregation to the porous in the bottom are reduced, which will increase the corrosion resistance. This illustrates the higher corrosion resistance of the sealed aluminum anodic oxide film than the unsealed one. [25]

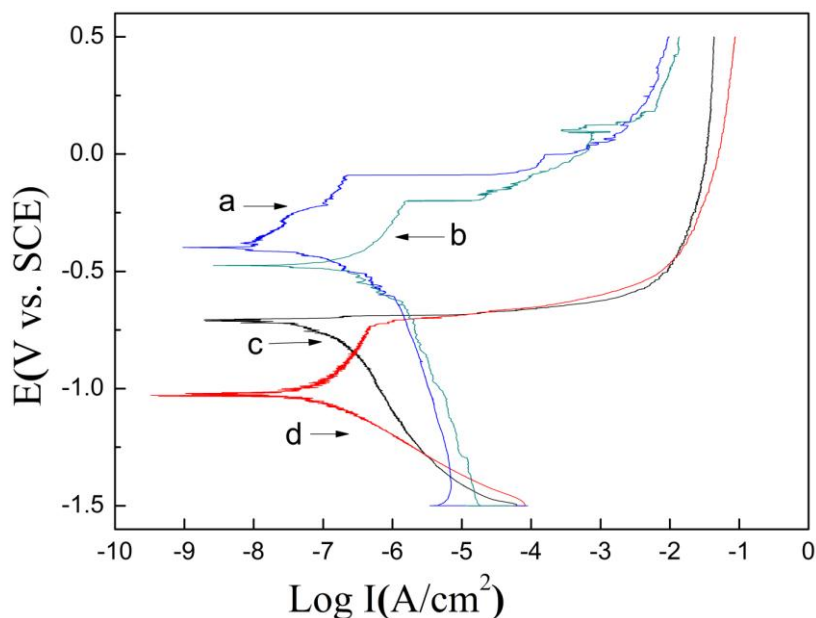


Figure 5. Polarization curves of anodic oxidation film with different scan rate after 20min of immersion in a 3.5wt. % NaCl solution (a)0.5mv/s (b)1mv/s (c)2mv/s(d)4mv/s. Temperature: 298K

The Fig.5 shows the corrosion potential of anodization film sealed by nickel and cobalt salt is changed gradually with different scan rate. Corrosion potential of the anodization film sealed by nickel and cobalt salt increases from -1.13V vs. Ag/AgCl to -0.40V vs. Ag/AgCl with scan rate decreases from 4mv/s to 0.5mv/s from the above results. On the other hand, the corrosion process of anodization film belongs to anode control, so corrosion resistance of the oxide film can be represented by the passive current density. As shown in the Fig.5, passive current increases from 10^{-1}A/cm^2 to 10^{-2}A/cm^2 with scan rate decreases from 4mv/s to 0.5mv/s. It indicated that corrosion of anodization film is significantly improved if corrosion current density decreases by a order of magnitude at the potential of anodization film.

3.1.3 Electrochemical impedance spectroscopy of anodic oxide film

Nyquist and Bode phase plots of the anodic oxidation film with different oxidation time are shown in Fig6. There are two time constants in the spectra obtained on the test from the Fig6a, as seen

from the Bode diagram, correspond to the two capacitors arc in Fig6b. The first constant appearing at high frequency represents electric double layer capacitor and the mass transfer resistance between the solution and 2024 Al. The second one appearing at low frequency represents the capacitance and resistance of anodization film under corrosion reaction. It can be seen from Fig6a, there is a certain difference in capacitance and resistance of the anodic oxide film under corrosion reaction at low frequency. The capacitance gradually reduced with an increase of oxidation time. The capacitance is $3.25 \times 10^{-5} \text{cm}^2 \text{s}^n \Omega$ calculated by equivalent circuit (table 2) in 30 minute. The capacitance then gradually increased when the oxidation time continues to increase. Capacitance becomes $4.31 \times 10^{-5} \text{cm}^2 \text{s}^n \Omega$ in 40 min oxidation time (table 2), but the change of the resistance value is not governed by any rule.

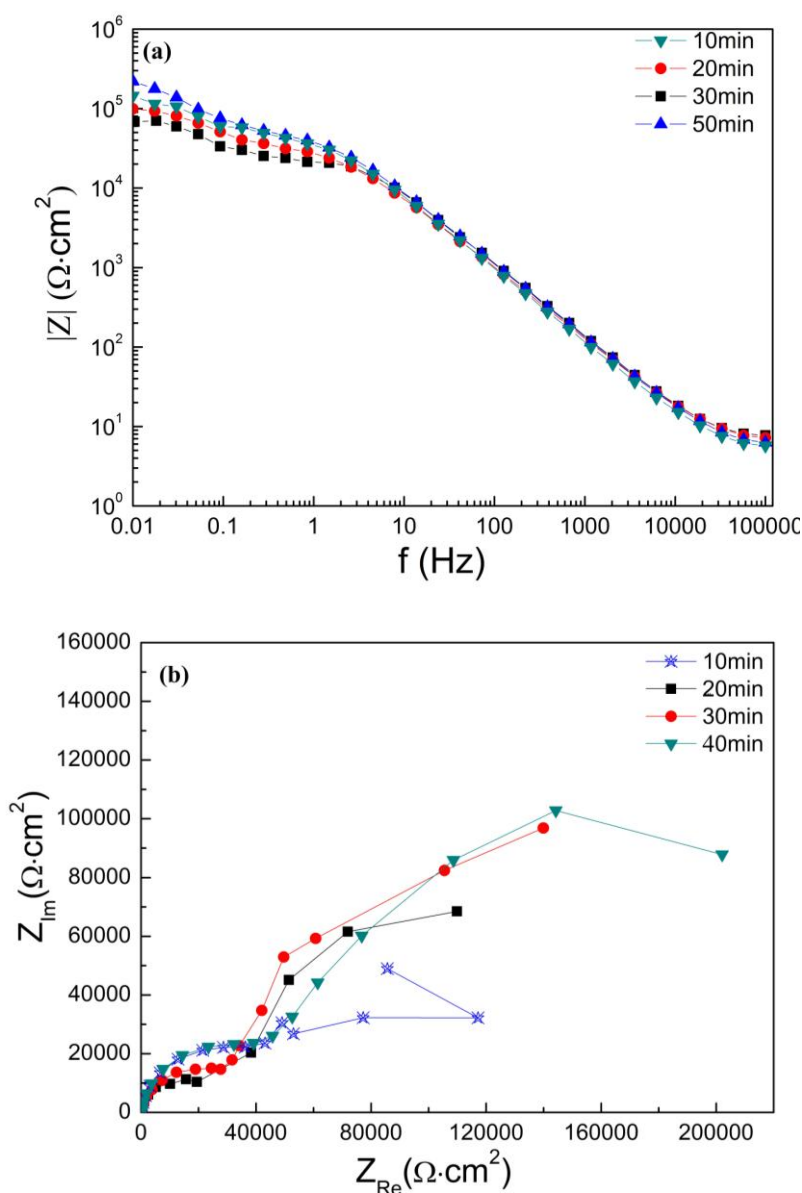


Figure 6. Nyquist (a) Bode phase (b) of anodic oxidation film with different oxidation time after immersed in a 3.5wt. % NaCl solution for 20min. Temperature: 298K

The double layer capacitance reached a maximum of $3.26 \times 10^{-6} \text{ (cm}^2\text{s}^n\Omega)$ in 20 min oxidation time. The capacitance value of the double layer will reduce again with increasing of oxidation time. The variation of R_t is consistent with that of the capacitance Q_p of the anodization film under corrosion reaction. The reason for this phenomenon is a complex issue. It may be related to the film thickness and pore size. Thicker oxidization films may prevent chloride ions diffusing into films. However, larger aperture of oxidization films would increase diffusion rate of chloride ions [25-27].

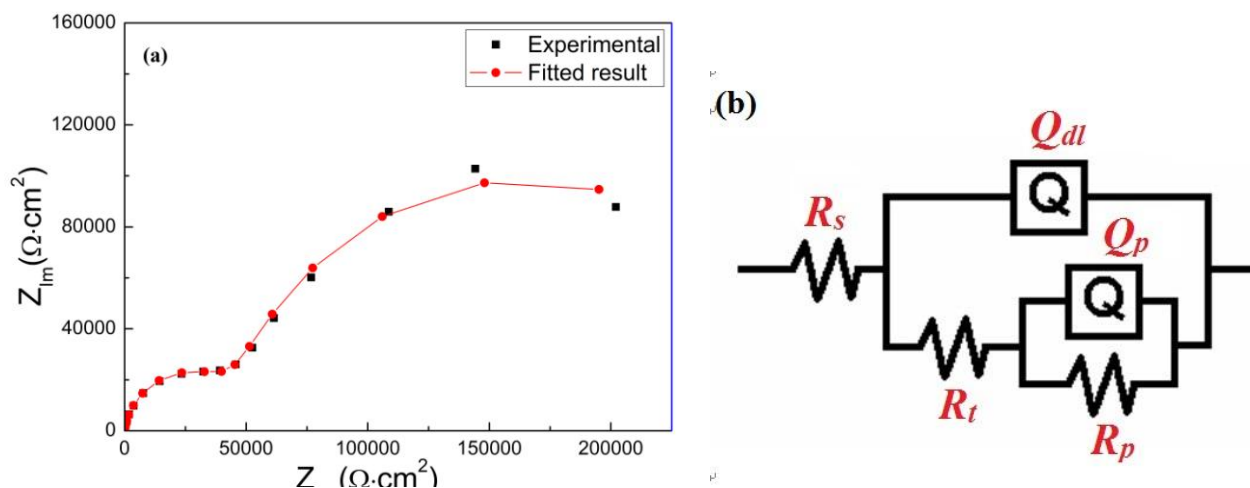


Figure 7. (a) Example of a fitted result for a selected EIS diagram(40min);(b)Equivalent circuit of 2024Al alloy immersed in 3.5wt. % NaCl solution (40min)

The experimental and calculated impedance results of sample are displayed in Fig. 7a. This figure represents that the data are well matched. Fig7b shows the schematic of this structure, which describes the electrochemical behavior of the system. The equivalent circuit that is reported in Fig. 7a is proposed here to model EIS results of the anodized layers on aluminum. This model was selected based on the circuits that were recommended for the anodic coating of aluminum by Moutarlier et al. [24]and Hoar and Wood[28].

Table 2. EIS data simulations for 2024Al alloy with aluminum anodic film in 3.5% NaCl solution.

Oxidation time (min)	Q_{dl} ($\text{cm}^2\text{s}^n\Omega$)	n	R_t (Ωcm^2)	Q_p ($\text{cm}^2\text{s}^n\Omega$)	n	R_p (Ωcm^2)
10	2.80×10^{-6}	0.92	4.13×10^4	3.73×10^{-5}	0.62	1.38×10^5
20	3.29×10^{-6}	0.89	3.33×10^4	3.38×10^{-5}	0.83	2.44×10^5
30	2.44×10^{-6}	0.80	2.61×10^4	3.25×10^{-5}	0.8	1.91×10^5
40	1.25×10^{-6}	1	4.58×10^4	4.31×10^{-5}	1	1.87×10^5

3.2 Morphology, microstructure and thickness of anodic oxidation film

3.2.1 Morphology, microstructure of anodic oxidation film

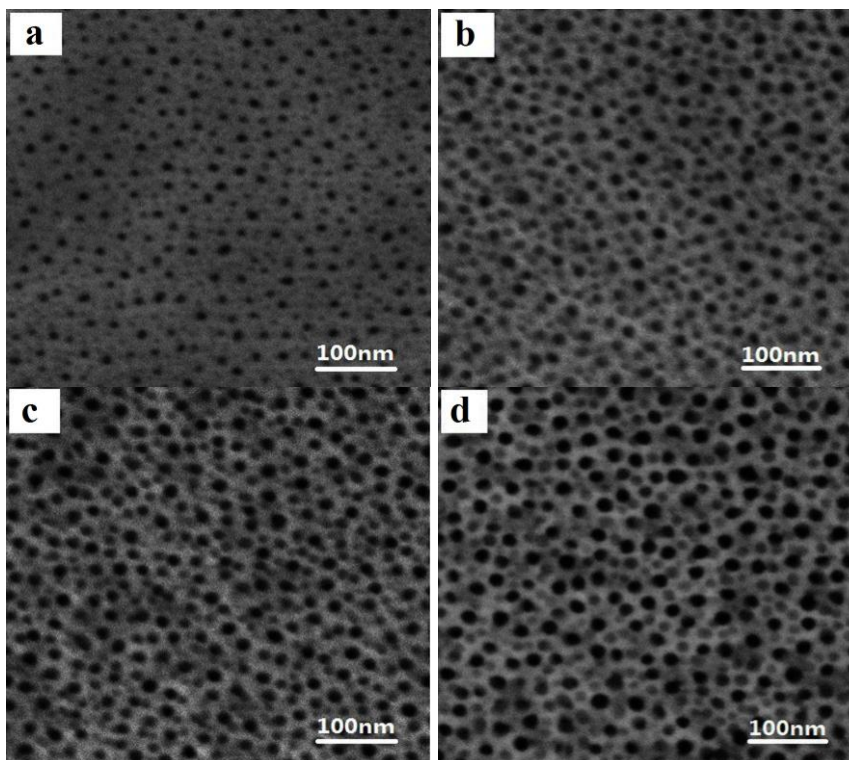


Figure 8. Surface morphologies of the anodic film for different time (a)10min;(b)20min;(c)30min;(d)40min

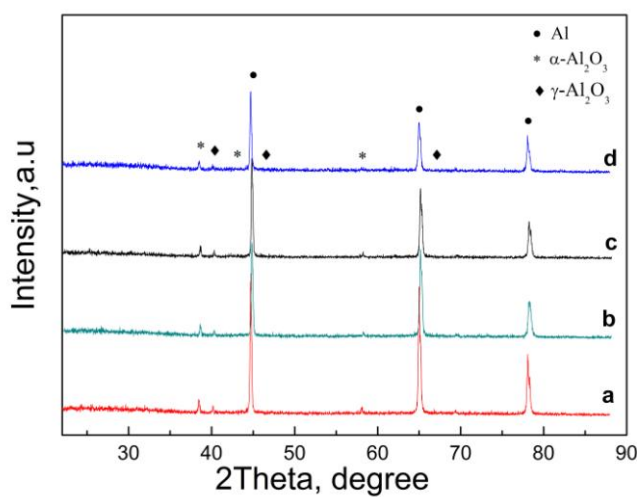


Figure 9. XRD pattern of anodic oxidation film formed on 2024 Al alloy under different oxidation time: (a) 10min; (b)20min; (c)30min; (d)40min.

Surface morphologies of the anodic oxide film under different time anodized in a solution of sulfuric acid and citric acid are shown in Fig.4a-d. The porous anodic aluminum oxide nanostructure is clearly seen and obtained under different oxidization time. Within the range of certain time, the pores size will increase gradually with the increase of oxidization time. This is because part of the porous in the connection and thus lead to greater holes under the voltage applied in the oxidation process.

Fig.9 shows the XRD pattern of the anodic oxidation film under different oxidation time. From the figure, the anodic oxidation film includes $\gamma\text{-Al}_2\text{O}_3$, $\alpha\text{-Al}_2\text{O}_3$ and a small amount of amorphous phase appeared at range 20° to 38° [26,29], which is in agreement with the study of Yerokhin [30]. Since the anodic oxidation film is not thick enough compared with the 2024 Al substrate, diffraction peaks of Al alloy substrate are reflected obviously in the XRD pattern.

3.2.2 Thickness and cross-section of the anodic oxidization film

Influences of different oxidization time on film thickness are described in Fig.10. It is found that there is a linear relationship between film thickness and oxidization time. Film thickness increases gradually with the rise on oxidization time. Generation and dissolution of oxidization film are two main processes during the anodic oxidization experimental. According to Fig.10, the thickness of film increases gradually in the range of 60 minutes. This result demonstrates that rate of oxidization film generation is faster than oxidization dissolution in the range of 60 minutes. However, longer oxidization time could induce to form bad quality films with rough surface. Upper left of Fig.10 gives the cross-sectional morphology of anodic oxidization film prepared for 30 minutes. The black area represents the anodic oxidization film (10 μm) which is coincided with the thickness measured by instrument.

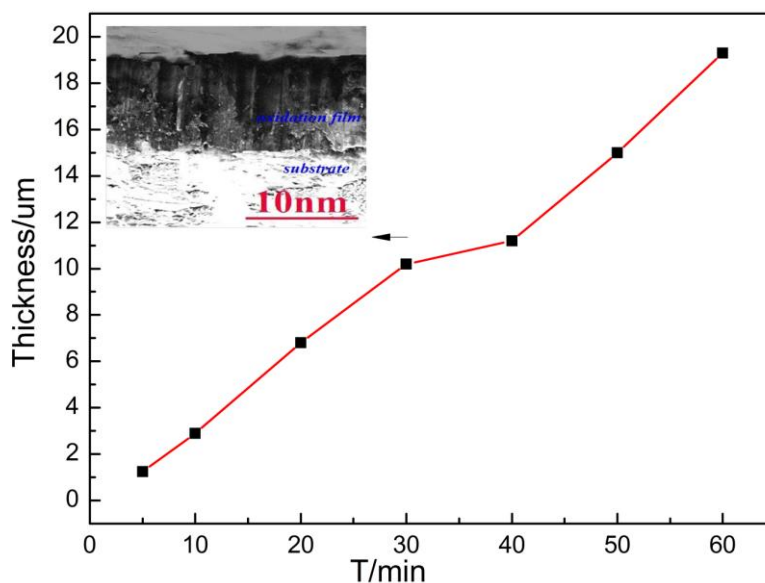


Figure 10. Thickness and cross-section (30min) of the anodic oxidization film under different oxidization time

4. CONCLUSION

Aluminum oxide films were prepared by anodic oxidation methods. Effects of oxidation time on chemistry properties, surface morphology and film thickness were investigated in the paper.

(1) According to polarization curves, samples obtained with different oxidation times show passivation phenomenon. Maintaining passivity current density is basically the same, but self-corrosion potential of anodized oxide films is different. Self-corrosion potential of anodized oxide films is more positive than substrate. Moreover, samples sealed by nickel and cobalt salts possess the most positive self-corrosion potential.

(2) Various impedance patterns of oxide films prepared with different times are observed. Impedance changes are not obvious in higher frequency condition, which indicate that double layer capacitor and transfer resistance between solution and substrate do not change significantly. However, impedance changes could be observed conspicuously in lower frequency region. It demonstrates that films' anti-corrosion capacity and resistance change significantly.

(3) With the increase of oxidation time, thickness and aperture of oxidized films increase gradually which induce to forming amorphous films.

ACKNOWLEDGEMENTS

This research was supported by the National Natural Science Foundation (No. 21171155), International Science and Technology cooperation Program of China (No.2011DFA52400) and Important Science and Technology innovation team of Zhejiang China (No.2010R50016).

References

1. S. Ono, M. Saito, H. Asoh, *Electrochim. Acta*, 51 (2005) 827
2. W. Lee, K. Schwirn, M. Steinhart, E. Pippel, R. Scholz, U. Gösele, *Nat. Nanotechnol.*, 3 (2008) 234
3. H. Masuda, F. Hasegawa, S. Ono, *J. Electrochem. Soc.*, 144(1997) L127
4. S. Ono, M. Saito, M. Ishiguro, H. Asoh, *J. Electrochem. Soc.*, 151 (2004) B473.
5. W. Lee, R. Ji, U. Gosele, K. Nielsch, *Nat. Mater.*, 5 (2006) 741.
6. X. Zhou, G.E. Thompson, G. Potts, *Trans. Inst. Met. Finish.* 78 (2000) 210.
7. M. Curioni, P. Skeldon, G.E. Thompson, J. Ferguson, *Proc. of the Adv. Mate. Res.*, 38 (2008) 48
8. M. Curioni, P. Skeldon, E. Koroleva, G.E. Thompson, J. Ferguson, *J. Electrochem. Soc.*, 156 (2009) C147
9. H.W. Wang, P. Skeldon, G.E. Thompson, *Tribology Transactions* 42 (1999) 202
10. M. Ward, D.R. Gabe, R.J. Latham, R.H. Dahm, *Trans. Inst. Met. Finish.*, 81(2003)122
11. M. Takaya, K. Hashimoto, Y. Toda, M. Maejima, *Surf. Coat. Technol.*, 169-167 (2003) 160
12. M. Maejima, K. Saruwatari, M. Takaya, *Surf. Coat. Technol.*, 132 (2000) 105
13. O. Jessensky, F. Müller, U. Gösele, *Appl. Phys. Lett.*, 72 (1998) 1173
14. C.-E. Barchiche, E. Rocca, C. Juers, J. Hazan, *J. Steinmetz, Electrochim. Acta*, 53(2007) 417
15. S. Mathieu, C. Rapin, J. Steinmetz, P. Steinmetz, *Corros. Sci.*, 45 (2003) 2741
16. A. Wendt, K. Weiss, A. Ben-Dov, M. Bamberger, B. Bronfin, *Magnesium Technology 2005 – TMS Annual Meeting*, San Francisco, USA(2005)
17. S. Mathieu, C. Rapin, J. Hazan, P. Steinmetz, *Corros. Sci.*, 44 (2002) 2737
18. C. Juers, E. Rocca, J. Steinmetz, *COM 2006: The Conference of Metallurgists – Symposium on Magnesium, Montréal, Canada(2006)*

19. H. Umehara, M. Takaya, S. Terauchi, *Mater. Sci. Forum*, 419–422 (2003) 883–888
20. L. Kouisni, M. Azzi, F. Dalard, S. Maximovitch, *Surf. Coat. Tech*, 192 (2005) 239
21. K.Z. Chong, T.S. Shih, *Mater. Chem Phys.* 80 (2003) 191
22. M. Zhao, S. Wu, J. Luo, Y. Fukuda, H. Nakae, *Surf. Coat. Tech*, 200(2006)5407
23. V.P. Parkhutik, V.I. Shershulsky, *J. Phys. D: Appl. Phys.* 25 (1992) 1258–1263
24. V. Moutarlier, M.P. Gigander, J. Pagetti, B.Normand, *Surf. Coat. Tech*, 161(2002) 267-274
25. Maysam Mohammadi, Ali Yazdani, Mohammad E. Bahrololoom, Akram Alfantazi, *J. Coat. Technol. Res*, 10(2)219-229, 2013
26. Lei Wen, Yaming Wang, Yu Zhou, Lixin Guo, Jia-Hu Ouyang, *Corros. Sci*, 53(2011)473-480
27. Lei Wen, Yaming Wang, Yu Zhou, Jia-Hu Ouyang, Lixin Guo, *Corros. Sc*, 52(2010)2687-2696
28. Hoar, TP, Wood,GC, *Electrochim.Acta*,7(1962)333-353
29. A.L.Vazquez, R.Carrera, E. Arce, N. Castillo, S. Castillo, *J. Alloys Compd*, 483(2009)418-421
30. A.L. Yerokhin, X. Nie,A. Leyland, A. Matthews, S.J. Dowey, *Surf.Coat.Technol.*122(1999)73